

An NMR analog of the quantum disentanglement eraser

G. Teklemariam[†], E. M. Fortunato[‡], M. A. Pravia[‡], T. F. Havel[‡], D. G. Cory[‡]

[†]*Department of Physics, MIT*

[‡]*Department of Nuclear Engineering, MIT*

We report the implementation of a three-spin quantum disentanglement eraser on a liquid-state NMR quantum information processor. A key feature of this experiment was its use of pulsed magnetic field gradients to mimic projective measurements. This ability is an important step towards the development of an experimentally controllable system which can simulate *any* quantum dynamics, both coherent and decoherent.

03.65.Bz, 03.67.-a, 03.67.Lx

One of the most intriguing effects in quantum mechanics is the “quantum eraser” [1–4]. Given an ensemble of identically prepared quantum systems, this effect is described by the *loss or gain* of interference in a subensemble that is determined by the outcome of the measurement of *one or the other* of a pair of noncommuting binary observables, respectively. Thus a quantum eraser demonstrates the principle of complementarity without making use of the corresponding uncertainty relation. Quantum erasers have previously been demonstrated by optical [5] as well as atom [6] interferometry. In this Letter we use liquid-state NMR spectroscopy on pseudo-pure states [7] to demonstrate a novel “disentanglement” eraser, due to Garisto and Hardy [8], in which not only interference, but also entanglement, is lost or gained in a subensemble. An analogous quantum erasure procedure operating on a pair of Bell states has recently been used by Zeilinger’s group to prepare an entangled three-photon state [9].

An important goal of our group is to design and build increasingly more powerful experimentally controllable devices capable of precisely simulating the *dynamics* of any quantum system with an equal or smaller Hilbert space dimension. Previously we have addressed the issues of coherent control [10] and pseudo-pure state preparation [11], and we are now developing methods for non-unitary quantum operations. The disentanglement eraser is of particular interest in this regard, because it allows us to show that NMR on pseudo-pure states is capable of reproducing even the decoherent dynamics associated with *strong* (projective) measurements on the members of the ensemble, which are needed to create or destroy entanglement in this eraser (cf. [11]).

It should be understood that the density matrices of the highly mixed macro-states involved in liquid-state NMR experiments can always be rationalized in terms of ensembles of disentangled micro-states [12]. Consequen-

tially, the ensemble-average observations on pseudo-pure states reported here do not prove the existence of the corresponding entangled micro-states in the sample. Nevertheless, because pseudo-pure states provide an equivalent representation of the underlying quantum *dynamics*, our experiments created exactly the same ensemble-average coherences that would have been observed if the same operations had been applied to the corresponding pure state ensemble, and this is sufficient for our purposes.

In the disentanglement eraser two of the spins (qubits) in a GHZ (Greenberger-Horne-Zeilinger) state [13,14] are regarded as the components of a Bell state labeled by the state of an additional “ancilla” spin #1 (left-most), i.e.

$$|\psi_{GHZ}\rangle = \frac{1}{\sqrt{2}}(|0\rangle|00\rangle + |1\rangle|11\rangle). \quad (1)$$

Assuming that the computational basis corresponds to the eigenvectors of the σ_z spin 1/2 operator, a projective measurement of the ancilla along z yields a mixture of separable states $|00\rangle$ and $|11\rangle$ labeled by the ancilla spin. This corresponds to the ensemble

$$\rho_z = E_+^1|00\rangle\langle 00| + E_-^1|11\rangle\langle 11|, \quad (2)$$

where $E_\pm^1 = \frac{1}{2}(I \pm \sigma_z^1)$ expresses the density matrices $|0\rangle\langle 0| \otimes \sigma_1 \otimes \sigma_1 = E_+^1$ and $|1\rangle\langle 1| \otimes \sigma_1 \otimes \sigma_1 = E_-^1$ in terms of the Pauli matrix $\sigma_z^1 \equiv \sigma_z \otimes \sigma_1 \otimes \sigma_1$, where $\sigma_1 = |0\rangle\langle 0| + |1\rangle\langle 1|$ and $I = \sigma_1 \otimes \sigma_1 \otimes \sigma_1$ is the 8×8 identity matrix.

Alternatively, expressing the GHZ state in terms of the x eigenstates of the ancilla spin and the Bell states of the other two spins yields

$$|\psi_{GHZ}\rangle = \frac{1}{\sqrt{2}}(|x_+\rangle|\phi_+\rangle + |x_-\rangle|\phi_-\rangle), \quad (3)$$

where $|x_\pm\rangle = (|0\rangle \pm |1\rangle)/\sqrt{2}$ and $|\phi_\pm\rangle = (|00\rangle \pm |11\rangle)/\sqrt{2}$. Thus a projective measurement along the x -axis followed by a rotation of the ancilla back to z gives

$$\rho_x = E_+^1|\phi_+\rangle\langle \phi_+| + E_-^1|\phi_-\rangle\langle \phi_-|. \quad (4)$$

This is a mixture of complementary Bell states each labeled by the state of the ancilla. Note that the partial trace over the ancilla in $|\psi_{GHZ}\rangle\langle \psi_{GHZ}|$, ρ_z and ρ_x are all equal to $(|00\rangle\langle 00| + |11\rangle\langle 11|)/2 = E_+^2 E_+^3 + E_-^2 E_-^3$, so that these states can be distinguished only if the information contained in the state of the ancilla is used.

These effects were demonstrated by liquid-state NMR using as the qubits the three spin 1/2 carbons in a ^{13}C -labeled sample of alanine ($\text{C}^1\text{O}_2^- - \text{C}^2\text{H}(\text{C}^3\text{H}_3) - \text{NH}_3^+$)

in deuterated water. With decoupling of the protons [16], this spin system exhibits a weakly coupled spectrum corresponding to the Hamiltonian

$$\mathcal{H}_{int} = \pi[\nu_1\sigma_z^1 + \nu_2\sigma_z^2 + \nu_3\sigma_z^3 + \frac{1}{2}(J_{12}\sigma_z^1\sigma_z^2 + J_{23}\sigma_z^2\sigma_z^3 + J_{13}\sigma_z^1\sigma_z^3)], \quad (5)$$

where the ν 's are Larmour frequencies and the J 's the spin-spin coupling constants in Hertz. The experiments were carried out on a Bruker AVANCE-300 spectrometer in a field of roughly 7.2 Tesla, where the resonant frequency of the second carbon is 75.4713562 MHz. The frequency shifts of the other carbons with respect to the second are 9456.5 Hz for the first one and -2594.3 Hz for the third, while the coupling constants are $J_{12} = 53.7$, $J_{23} = 34.6$ and $J_{13} = -1.4$ Hz. The T_1 relaxation times for the three spins are 21, 2.5 and 1.6 s, while the T_2 times are 550, 420 and 800 ms, respectively.

The pseudo-pure ground state was prepared from the thermal equilibrium state by the procedure summarized in Table 1, which uses magnetic field gradients (denoted by $[\nabla]$) to dephase off-diagonal elements of the density matrix at strategic points along the way [7]. Letting $\hat{\rho}_{eq} = \sigma_z^1 + \sigma_z^2 + \sigma_z^3$ be the traceless part of the equilibrium density matrix (with all physical constants set to unity), the first two transformations in the table yield the state $(\sqrt{3}/\sqrt{32})\sigma_z^2 + (\sigma_z^1 + \sigma_z^3)E_+^2$. Spins 1 and 3 may then be transformed into the state $(\sqrt{3}/\sqrt{32})(\sigma_z^1 + \sigma_z^3 + \sigma_z^1\sigma_z^3)$ by the efficient two-spin pseudo-pure state preparation procedure described in Ref. [11] (Eq. (47)), yielding the three-spin pseudo-pure ground state

$$\hat{\rho}_{ini} = \frac{\sqrt{3}}{\sqrt{32}}(E_+^1 E_+^2 E_+^3 - \frac{1}{8}) \equiv (|000\rangle\langle 000| - \frac{1}{8}). \quad (6)$$

The logic network shown in Fig. 1 transforms this state into the pseudo-pure GHZ state, and then decoheres the ancilla as indicated. The GHZ state is obtained by rotating spin 2 (since $J_{13} \ll J_{12}, J_{23}$) to the x axis in the rotating frame with a $\pi/2$ y -rotation $R_y^2(\pi/2) \equiv \exp(-i\sigma_y^2\pi/4)$, and then using it as the control for a pair of c-NOT (controlled-NOT [18]) gates to the other two spins. This pair of c-NOT's was implemented by the propagator $N^{13|2} \equiv e^{i(\sigma_x^1 - \sigma_x^3)E_+^2\pi/2} = e^{i\sigma_x^1 E_+^2\pi/2} e^{-i\sigma_x^3 E_+^2\pi/2}$ (ensuring cancellation of the phases $\pm i$ between the two factors). The overall sequence of transformations on the corresponding state vector is thus:

$$\begin{aligned} |000\rangle &\xrightarrow{R_y^2(\pi/2)} |0\rangle(|0\rangle + |1\rangle)|0\rangle/\sqrt{2} \\ &\xrightarrow{N^{13|2}} (|000\rangle + |111\rangle)/\sqrt{2} \equiv |\psi_{GHZ}\rangle \end{aligned} \quad (7)$$

Implementations of these operations in NMR by RF (radio-frequency) pulse sequences may be found in Refs. [7,11,19]. The resulting pseudo-pure GHZ state is written in product operator notation as [19]

$$\hat{\rho}_{GHZ} = \frac{\sqrt{3}}{4\sqrt{2}}(\sigma_z^1\sigma_z^2 + \sigma_z^2\sigma_z^3 + \sigma_z^1\sigma_z^3 + \sigma_x^1\sigma_x^2\sigma_x^3 - \sigma_y^1\sigma_y^2\sigma_y^3 - \sigma_x^1\sigma_y^2\sigma_y^3 - \sigma_y^1\sigma_x^2\sigma_y^3), \quad (8)$$

and has previously been studied by NMR in Refs. [20,21].

The coherences of ρ_{GHZ} can be dephased, exactly as they would be by strong measurements of σ_z on all the individual systems in the ensemble, by means of magnetic field gradients similar to those used to prepare the initial pseudo-pure state (cf. [11]). Specifically, a constant gradient $\nabla = \partial B_z/\partial z$ applied for a period t along the static field axis z causes spin evolution under the Hamiltonian $z\gamma\nabla\frac{1}{2}\sum_{j=1}^3\sigma_z^j$, where γ is the gyromagnetic ratio of all the spins. This multiplies each coherence $\rho_{k\ell}$ ($k \neq \ell$) with a spatially dependent phase $\exp(-i\gamma m_{k\ell}\nabla zt/2)$, where $m_{k\ell}$ is the *coherence order* [22] (i.e. the difference in the z -component of the angular momentum in units of \hbar between the $|k\rangle$ and $|\ell\rangle$ states [16]). Thus after such a gradient pulse the density matrix averaged over the sample volume satisfies $\rho_{k\ell} = 0$ for all $k \neq \ell$ save for the zero quantum coherences ($m_{k\ell} = 0$). Because only one spin is dephased in the eraser experiments, only single quantum coherences are of consequence.

This dephasing operation was made specific to those coherences involving transitions of the ancilla spin 1 by applying a π pulse to the other two spins, after which a second gradient pulse of the same amplitude and duration ‘‘refocuses’’ all the other coherences. At the same time it is necessary to also refocus the evolution under the internal Hamiltonian using π pulses selective for single spins. A sequence of RF and gradient pulses which accomplishes this is (in temporal order):

$$\begin{aligned} P_z^1 &= [\nabla]_z - [\pi]_x^2 - [\nabla]_z - [\pi]_x^{2,3} - \\ &[\nabla]_z - [\pi]_{-x}^2 - [\nabla]_z - [\pi]_{-x}^{2,3} \end{aligned} \quad (9)$$

The corresponding effective (average) propagator is simply $e^{-i\nabla z\sigma_z^1/2}$. This dephases the ancilla spin in the same way as would a strong measurement of σ_z^1 on every member of the ensemble. To dephase the ancilla in the same way as would a strong measurement of σ_x^1 , one need only rotate the ancilla to the z -axis with a $\pi/2$ y -rotation $R_{-y}^1(\pi/2)$, as follows:

$$P_x^1 = [\pi/2]_{-y}^1 - P_z^1 \quad (10)$$

The ancilla is left along z for subsequent tomography.

The results of P_z^1 and P_x^1 applied to $\hat{\rho}_{GHZ}$ are

$$\hat{\rho}_{GHZ} \xrightarrow{P_z^1} \frac{\sqrt{3}}{4\sqrt{2}}(\sigma_z^1\sigma_z^2 + \sigma_z^2\sigma_z^3 + \sigma_z^1\sigma_z^3), \quad (11)$$

$$\hat{\rho}_{GHZ} \xrightarrow{P_x^1} \frac{\sqrt{3}}{4\sqrt{2}}(\sigma_z^2\sigma_z^3 + \sigma_z^1\sigma_x^2\sigma_x^3 - \sigma_z^1\sigma_y^2\sigma_y^3). \quad (12)$$

These states were confirmed by full tomography [17]. Because only the single quantum ($m_{k\ell} = 1$) coherences give rise to observable (dipolar) magnetization, it is necessary

to collect spectra not only following the dephasing operation, but also following additional $\pi/2$ pulses selective for single spins, to rotate the $m_{kl} = 0$ and $m_{kl} > 1$ coherences, as well as the populations (diagonal elements), into observable single quantum coherences. Tomography was performed at the points of the procedure indicated in Fig. 1; the real parts of these four density matrices are shown in Fig. 2 (the imaginary parts were essentially zero).

The overall precision of quantum information transmission was quantified by an extension of Schumacher’s fidelity [23], which takes into account not only systematic errors, but also the net loss of magnetization due to random errors. This measure, called the *attenuated correlation*, is given by

$$c(\hat{\rho}^{exp}) = \frac{Tr(\hat{\rho}^{the} \hat{\rho}^{exp})}{Tr(\hat{\rho}^{the} \hat{\rho}^{the})}. \quad (13)$$

Here, $\hat{\rho}^{the}$ is the measured pseudo-pure ground state $\hat{\rho}_{ini}^{exp}$, transformed on a computer by the same sequence of unitary and non-unitary (measurement) operations to which it was subjected on the spectrometer to get $\hat{\rho}^{exp}$. Note that, since $Tr(\hat{\rho}^{exp} \hat{\rho}^{exp}) \leq Tr(\hat{\rho}^{the} \hat{\rho}^{the})$, the Cauchy-Schwarz inequality implies that $-1 \leq c(\hat{\rho}^{exp}) \leq 1$.

The values of the correlation for each of the four tomographic readouts were $c(\hat{\rho}_{ini}^{exp}) = 1$ (by definition), $c(\hat{\rho}_{GHZ}^{exp}) = 0.88$, $c(\hat{\rho}_z^{exp}) = 0.92$ and $c(\hat{\rho}_x^{exp}) = 0.93$. Although not included here for brevity, tomography on the state $|0\rangle(|00\rangle + |11\rangle)/\sqrt{2}$ yields an attenuated correlation of 0.93, showing that spins 2 and 3 were entangled before the GHZ state was created. The increases in c are not unexpected, since the additional π and gradient pulses needed to mimic measurements on ρ_{GHZ} are easily implemented with high precision, and the tomographic errors are estimated at $\pm 5\%$. The leading candidates for the loss of correlation are pulse imperfections arising from RF field inhomogeneity, less than perfect RF pulse calibrations, and relaxation. The total time before data collection in the complete experiments was ca. 65 ms; the time required to prepare the GHZ state from the initial state was 21 ms. Since the T_2 relaxation times of the spins varied from 400 – 800 ms, the net loss of magnetization due to relaxation in going from $\hat{\rho}_{ini}$ to $\hat{\rho}_{GHZ}$ was 3 – 5%. Thus, the additional loss due to pulse imperfections etc. was about another 5% or so, confirming the high precision of the strongly modulated pulse sequences used in these experiments.

In conclusion, we have used a three-spin liquid-state NMR quantum information processor to obtain a high-precision implementation of the dynamics, both coherent and decoherent, underlying Garisto and Hardy’s “disentanglement eraser”, and have found that the experimental results confirm the theoretically predicted conditional expectation values. This shows that we can judiciously

and selectively render phase information macroscopically inaccessible in a way that precisely mimics the decoherence attendant on strong measurements. It should be noted that during this dephasing operation all interactions among the spins were refocused, and that only the *macroscopically accessible* information contained in the ancilla spin due to its earlier interactions with the other two was changed. This was nevertheless sufficient to convert the net triple-quantum coherence in ρ_{GHZ} into a pair of double-quantum coherences, conditional on the state of the ancilla representing this information. Unlike previous eraser implementations, it was not necessary to explicitly read out this information in each member of the ensemble in order to see the conditional coherence, because this was done for us by the coupling of the ancilla to the other two spins while the spectra were being measured. This ability to convert macroscopic correlations into one another via well-defined microscopic (molecular) interactions is the essence of ensemble quantum computing.

We thank L. Viola and S. Somaroo for helpful discussions. This work was supported by the U.S. Army Research Office under grant number DAAG 55-97-1-0342 from the Defense Advanced Research Projects Agency.

Correspondence should be addressed to DGC (email:dcory@mit.edu).

-
- [1] E. T. Jaynes, *Foundations of Radiation Theory and Quantum Electrodynamics*, A. O. Barut, ed., Plenum Press, New York and London (1980).
 - [2] M. O. Scully and K. Druhl, *Phys. Rev. A* **25**, 2208 (1982); M. O. Scully, B. G. Englert and H. Walther, *Nature* **351** (6322) 111-116 (1991); M. O. Scully and M. S. Zubairy, *Quantum Optics*, Cambridge Univ. Press (1997).
 - [3] P. G. Kwiat, A. M. Steinberg and R. Y. Chiao *Phys. Rev.* **49** (1) 61-68 (1994); T. J. Herzog, P. G. Kwiat, H. Weinfurter and A. Zeilinger, *Phys. Rev. Lett.* **75** (17) 3034-3037 (1995); P. G. Kwiat, P. D. D. Schwindt and B.-G. Englert, *Mysteries, Puzzles and Paradoxes in Quantum Mechanics*, ed. R. Bonifacio, AIP (1999).
 - [4] J. M. Raimond, M. Brune and S. Haroche, *Phys. Rev. Lett.* **79**, 1964-1967 (1997).
 - [5] P. G. Kwiat, A. M. Steinberg and R. Y. Chiao, *Phys. Rev. A* **45** 7729-7739 (1992).
 - [6] S. Dürr, T. Nonn and G. Rempe, *Nature* **395**, 33-37 (1998).
 - [7] M. D. Price, T. F. Havel and D. G. Cory, *Physica D* **120**, 82-101 (1998).
 - [8] R. Garisto and L. Hardy, *Phys. Rev. A* **60**, 827-831 (1999).
 - [9] D. Bouwmeester, J.W. Pan, M. Daniell, H. Weinfurter and A. Zeilinger *Phys. Rev. Lett.* **82** 1345-1349 (1999).
 - [10] D.G. Cory, R. Lafamme, E. Knill, L. Viola, T.F. Havel, N. Boulant, G. Boutis, E. Fortunato, S. Lloyd, R. Mar-

- tinez, C. Negrevergne, M. Pravia, Y. Sharf, G. Teklemariam, Y.S. Weinstein and W.H. Zurek, *Fort. Phys.* **48**, 875-907 (2000).
- [11] T. F. Havel, S. S. Somaroo, C. H. Tseng and D. G. Cory, *Appl. Alg. Eng., Commun. Comput.* **10** 339-374 (2000).
- [12] S. L. Braunstein, C. M. Caves, R. Jozsa, N. Linden, S. Popescu and R. Schack, *Phys. Rev. Lett.* **83**, 1054-1057 (1999).
- [13] D. M. Greenberger, M. A. Horne, A. Shimony, A. Zeilinger, *Am. J. Phys.* **58**, 1131-43 (1990)
- [14] D. Mermin, *Am. J. Phys.* **58**, 731-4 (1990)
- [15] S. Lloyd, *Phys. Rev. A* **57**, 1473-1476 (1998).
- [16] R. Freeman, *Spin Choreography*, Oxford Univ. Press, Oxford, UK (1998).
- [17] I. L. Chuang, L. M. K. Vandersypen, X. Zhou, D. W. Leung and S. Lloyd, *Nature* **393**, 143-146 (1998).
- [18] A. Steane, *Rept. Prog. Phys.* **61**, 117-173 (1998).
- [19] S. S. Somaroo, D. G. Cory and T. F. Havel, *Phys. Lett. A* **240**, 1-7 (1998).
- [20] R. J. Nelson, D. G. Cory and S. Lloyd, *Phys. Rev. A* **61**, 022106 (2000).
- [21] R. Laflamme, E. Knill, W. Zurek, P. Catasti and S. Mariappan, *Phil. Trans. Roy. Soc. Lond. A* **356**, 1941-1948 (1998).
- [22] A. Sodickson and D. G. Cory, *Prog. NMR Spect.*, **33**, 77-108 (1998).
- [23] B. Schumacher, *Phys. Rev. A* **54**, 2614-2628 (1996).

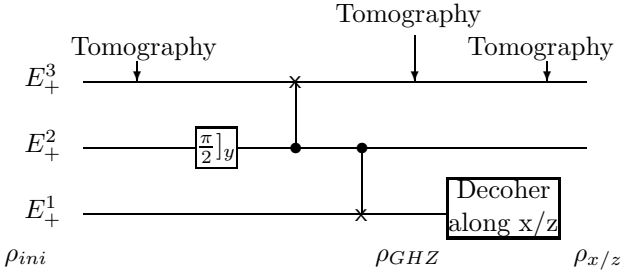


FIG. 1. Logic network for the disentanglement eraser. Initially, a pseudo-pure state on spins 1, 2 and 3 is created, $\rho_{ini} = |000\rangle\langle 000| \equiv E_+^1 E_+^2 E_+^3$. A $\frac{\pi}{2} y$ -pulse is then applied to spin 2, followed by two controlled-not (c-NOT) gates to create the GHZ state (see text). Conditionality on the second spin being in the $|1\rangle$ state is represented in the network by a filled circle on its time line. Finally, the two complementary measurements, σ_z^1 and σ_x^1 , are applied to spin 1. State tomography was performed to fully reconstruct the density matrices at the positions indicated.

Transformations

- 1) $[\nabla] e^{-\frac{i}{2} \cos^{-1}(\frac{\sqrt{3}}{4\sqrt{2}}) \sigma_x^2}$
- 2) $[\nabla] e^{-i\frac{\pi}{4}(\sigma_y^1 + \sigma_y^3) E_+^2}$
- 3) $e^{i\frac{\pi}{4} \sigma_x^1} e^{-i\frac{\pi}{4} \sigma_z^1 \sigma_z^2} e^{-i\frac{\pi}{4}(\sigma_y^1 + \sigma_y^2)} e^{-i\frac{\pi}{4} \sigma_z^1 \sigma_z^2} e^{-i\frac{\pi}{4} \sigma_x^2}$
- 4) $[\nabla] e^{i\frac{\pi}{12}(\sigma_y^2 + \sigma_y^3)} e^{-i\frac{\pi}{4} \sigma_z^1 \sigma_z^2} e^{-i\frac{\pi}{8}(\sigma_x^2 + \sigma_x^3)}$

TABLE I. This table shows the transformations used to obtain the initial state from the thermal state, ρ_{eq} .

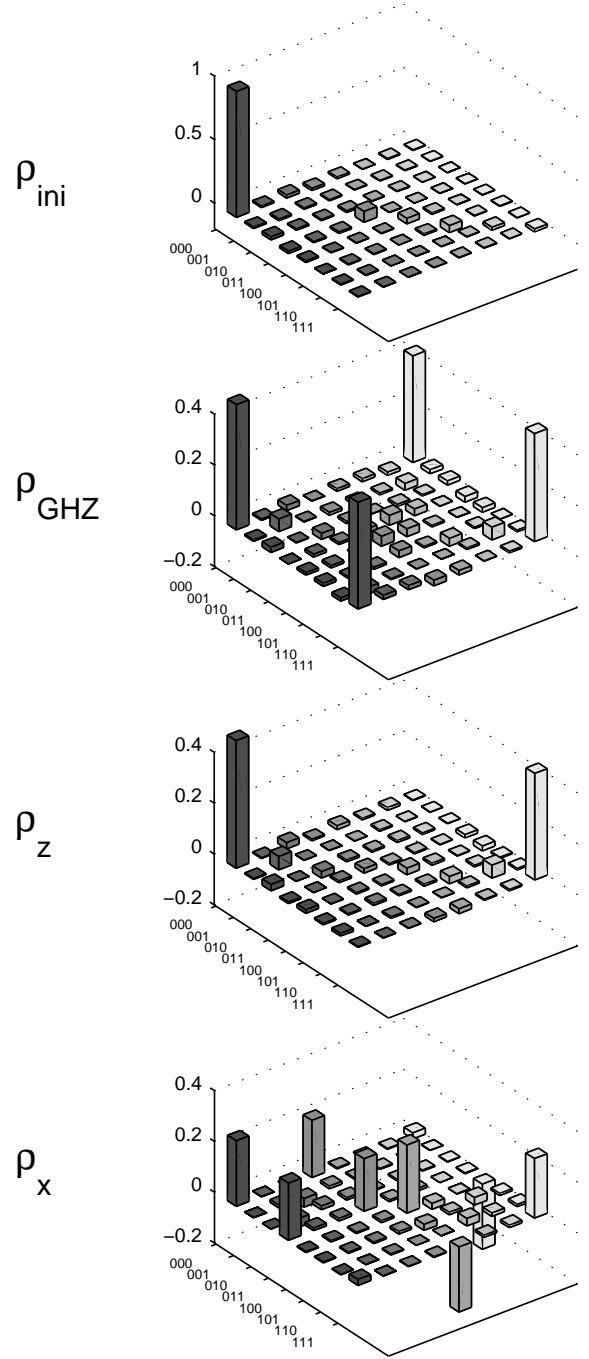


FIG. 2. Experimental density matrices reconstructed by tomography (in normalized units). The rows are enumerated in the standard computational basis, where for example 000 represents the state label $|000\rangle$. Although not shown, the columns are similarly labeled with the leftmost end representing $|000\rangle$ and the rightmost end representing $|111\rangle$. ρ_{ini} is the three-spin pseudo-pure ground state, and ρ_{GHZ} is the pseudo-pure GHZ state. The last two plots are ρ_z , which is ρ_{GHZ} after decohering spin 1 about the z -axis, and ρ_x , which is after decohering it about the x -axis. (Note: ρ_{GHZ} , ρ_z and ρ_x have been magnified by a factor of two for clarity). An amount of identity, chosen to optimize the input projection, was added to all experimentally measured density matrices.